Materials Science & Engineering C 104 (2019) 109862

Contents lists available at ScienceDirect

Materials Science & Engineering C

journal homepage: www.elsevier.com/locate/msec

Antibacterial properties of nanoporous graphene oxide/cobalt metal organic framework

Shadie Hatamie[a,b,*], Mohammad Mahdi Ahadian[c], Mahsa Soufi Zomorod[d], Shukoofeh Torabi[d], Ali Babaie[e], Simzar Hosseinzadeh[f], Masoud Soleimani[g], Niloofar Hatami[h], Zung-Hang Wei[a,b,*]

[a] Institute of NanoEngineering and MicroSystems, National Tsing Hua University, Hsinchu 30013, Taiwan
[b] Department of Power Mechanical Engineering, National Tsing Hua University, Hsinchu 30013, Taiwan
[c] Institute for Nanoscience and Nanotechnology (INST), Sharif University of Technology, Tehran, Iran
[d] Stem Cell Technology Research Center, Tehran, Iran
[e] Faculty of New Sciences and Technologies, University of Tehran, Tehran, Iran
[f] Department of Tissue Engineering and Applied Cell Science, School at Advance Technology in Medicine, Shahid Beheshti University of Medical Sciences, Tehran, Iran
[g] Department of Hematology, Faculty of Medical Sciences, Tarbiat Modares University, Tehran, Iran
[h] Department of Ophthalmology, University of Cologne, Cologne, Germany

ARTICLE INFO

Keywords:
Metal-organic framework
Graphene oxide
Cobalt
Antibacterial activity

ABSTRACT

Metal-organic framework (MOF) based graphene oxide (GO) recently merits of attention because of the relative correspondence of GO with metal ions and organic binding linkers. Furthermore, introducing the GO to the Co-MOF to make a new nanoporous hybrid have are improved the selectivity and stability of the Co-MOF. Here the graphene oxide/cobalt metal organic framework (GO/Co-MOF) was synthesized by a solvothermal process using cobalt salt and terephthalic acid and used for biocidal activity, against the growth of the Gram-negative *Escherichia coli* and Gram-positive *Staphylococcus aureus* bacteria. X-ray diffraction, Fourier transform infrared spectroscopy and Raman spectroscopy were confirmed the successful synthesize of metal organic framework and incorporation of Co-MOF in to GO sheets. Scanning electron microscopy was showed the cornflower structure of GO/Co-MOF, and transmission electron microscopy was confirmed, the Co-MOF are decorated on GO. Cytotoxicity study of GO/Co-MOF using 3-[4,5-dimethylthiazol-2yl]-2,5-diphenyltetrazolium bromide (MTT) cell viability assay showed the biocompatibility to human fibroblasts cell over 72 h. The growth inhibition of the *Escherichia coli* and *Staphylococcus aureus* bacteria are reached over 99% for bacteria concentration of 100 μg/mL. The excellent antibacterial activity of GO based Co-MOF is linked to synergistic effect of sharp edges of the GO sheets and the toxic effect of cobalt ions (Co^{2+}) which are released from their surfaces. The GO/Co-MOF radical scavenging assay was measured using 1,1-diphenyl-2-picrylhydrazyl (DPPH) antioxidant assay for samples incubated with cells which confirmed the minimum radicals' toxicity on bacteria. This novel graphene oxide based MOF with its intrinsic superior porous structure, highly active metal coordination, and commercial linker, is an excellent promising candidate to use in biological and pharmaceutical applications as high potential sustained bactericidal materials.

1. Introduction

Metal-organic frameworks (MOFs) are highly porous crystalline materials with great loading capacity, structure variety, and biodegradability, which recently have merit of attention to be used across biological and medical applications [1–5].

MOFs are a new class of inorganic-organic hybrid crystalline porous materials, which metal ions act as coordination centers and organic ligands act as linkers between the metal centers [6]. Chemical properties, large surface area, and tunable pore sizes of MOFs make them applicable as catalysts [7,8], chemical/bio sensors [9,10], drug delivery [11,12], hydrogen storage [13], antimicrobial activity [14–18], and super capacitor [19] etc.

The growing of the multi resistant pathogens against antibiotic therapy has occurred the problem for the human health care. There are traditional sterilized treatments, which have mainly applied chemical agents like as ethanol, phenol for cleansing hands and surfaces which have not the long term stability [20]. Furthermore, using of gamma and

* Corresponding authors at: Institute of NanoEngineering and MicroSystems, National Tsing Hua University, Hsinchu 30013, Taiwan.
E-mail addresses: hatamie@mx.nthu.edu.tw (S. Hatamie), wei@pme.nthu.edu.tw (Z.-H. Wei).

https://doi.org/10.1016/j.msec.2019.109862
Received 12 September 2018; Received in revised form 15 May 2019; Accepted 3 June 2019
Available online 15 June 2019
0928-4931/

ultraviolet irradiation, and ozone treatment are created toxic by-products [21,22]. Among with them, silver metal and silver nanoparticles (NPs) are of attention for antimicrobial efficiency against Gram negative and Gram positive bacteria cells. While using the silver as the disinfection agent are too costly, and there is limitation of using it in higher amount while its expensive and better to not use in a corrosive atmosphere [23]. But cobalt is not expensive element and it has also high antibacterial activity [24–27].

Then the novel idea was to cover silver NPs with metal oxide such as titanium dioxide (TiO_2), which is reducing the expense of silver while using small dosage of it, and increases the surface area and gives the silver long term stability [28]. However, MOFs, which have structured of metal atoms like as metal/metal oxide NPs have shown strong and efficient antibacterial activity because of their long term stability and their inherent active centers which are stabilized via chemical bonds formation which making the MOFs to be giant material with strong formation which are affective to inactive bacteria through rupture of their lipid membrane [29]. However, the antimicrobial activity of MOFs is corresponding to the type of metal in MOF structure, which can used for storage of metal ions and release them gently as an great advantages with compared to the metal/metal oxide NPs [30,31]. The MOFs have ability to sustained release of metal and prevent their oxidation and avoid their agglomeration [32]. In addition, different active ligands and/or biological ligands can be used to build MOFs [33]. Furthermore, there have been several report on antimicrobial activities of cobalt based MOFs, S. Aguado et al. presented antibacterial activity of cobalt base MOFs using imidazolates linkers (ZIF-67 with 2-methylimidazolate and Co-SIM-1 with 4-methyl-5-imidazolecarboxaldehyde as linkers) which make zeolite structures [34], and polymer based Ag [AgTAZ]. Their determined the cobalt-imidazolates shows higher antibacterial activity against three bacteria types (*S. cerevisiae*, *Pseudomonas putida*, and *E. coli*) even higher than for Ag TAZ. Their results show the release of the Co^{2+} ions in bacteria solution for both cobalt-MOFs. In another research work, the antibacterial activity of cobalt –based MOF (Co-TDM) was done against *E. coli* bacterial which results shows better antimicrobial activity for cobalt-based MOF in compare to the Ag NPs. The cobalt-based MOF shows the inhabitation of bacterial via lipid peroxidation and disruption of the bacteria cell walls [35]. Also, it is demonstrating that transition metal ions (Cu^{2+}, Zn^{2+}, Mn^{2+}) based MOF could inhibit growth of bacteria by release of metal ions in bacterial solution [5,36]. However, there are some defect on using MOFs, which is regarding to their low order proficiency at electrical conduction, electrochemistry and have an inferior capability of stability [37,38]. Attention to such a defect, it would be necessary to make MOF-based composites and installation of the MOFs with various materials depended on the final composites gain application. In this research work, the hybrid of the GO and the Co-MOFs are synthesized to combine the benefit of the both source of these composite on bacteria inhibition.

GO is a sp^2 hybridized sheet with aromatic structure of carbon atoms which has delocalized surface π-electrons, and reactive oxygen functionalized group, which is applicable to use in thermal, mechanical, electrical and biomedicine [39–45]. The composites based on GO and nanomaterials and further MOFs are in attention because of their extraordinary improvements in their electrical and mechanical properties, their better stability, avoid of their agglomeration and improve hydrophilicity in aqueous medium [46]. There are several works were reported on anti-biocidal activity of GO-based NPs, these studies majorly focus on GO based composites such as magnetic GO [47,48], GO/Ag [49,50], GO/TiO2 [51]. The antibacterial activity of GO was proved to be due to the physical damage of cell membrane by the sharp edges of their sheets, which causes loss of bacterial membrane integrity, RNA leakage and oxidative stress [51]. Zhang et al. investigated the antibacterial and antibiofouling properties of the GO deposited on the polyampholyte hydrogel for waste water treatments [52]. They prove that polymer membrane contained with GO, avoided the forming of the

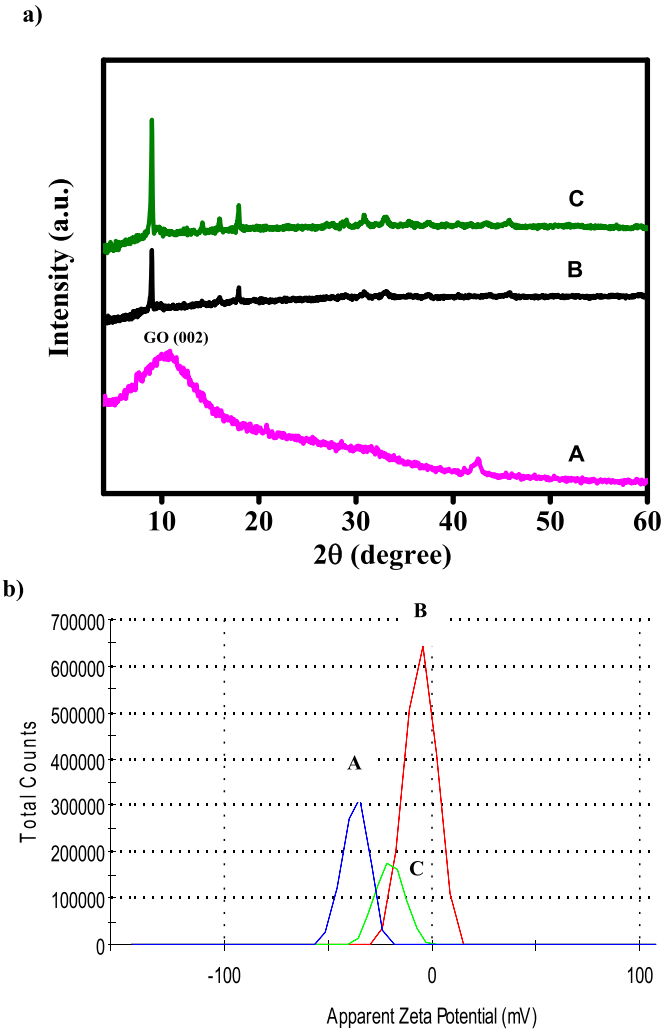

Fig. 1. (a) XRD pattern and (b) zeta potential of GO (A), Co-MOF (B) and GO/Co-MOF (C) samples.

biofilm. The results shown that GO-P-PES membrane are killed 80% of the *E. coli* bacteria which deposited in their surfaces compared to the PES and p-PES membrane. The Shuai et al. was introduced GO-Ag in the PLLA-PGA scaffold to increase the scaffold mechanical properties using GO and antibacterial activities using Ag NPs. They are discovered which introducing the Ag in the GO was reduced the aggregation of the Ag NPs. In this paper the antibacterial activity are done on *E. coli* ATCC-25922 bacterial cells. The maximum antibacterial activity is reported to be 95% for 1 wt% of GO-Ag/scaffold. The authors explain that the antibacterial possible mechanism are corresponding to the capturing effect of GO nano sheets and killing effect of Ag NPs [53]. Recently, there are several reports on benefits for make GO/Co-MOFs nano hybrid to improve Co-MOFs stability through the effect of graphene based materials as template [54]. In GO/Co-MOFs combination by adding of the graphene-based materials in MOF, the ionic groups and the aromatic sp^2 domains of GO could occurred the bonding interactions to MOFs and the GO carboxylate groups can guide the MOFs growth and could increase the coordination bonding [37]. The graphene-based/MOF materials can also positively affect the MOFs properties such as enhanced their dispersion [55], diminish aggregation [56], enlarge their specific surface area [57], increase their available active sites [58], and accelerate their electron transfer [59].

Herein, the novel graphene oxide/cobalt-MOF is synthesized using solvothermal method using commercial and cheap ligand. The superior antibacterial activity of the GO/Co-MOF hybrid on Gram positive and

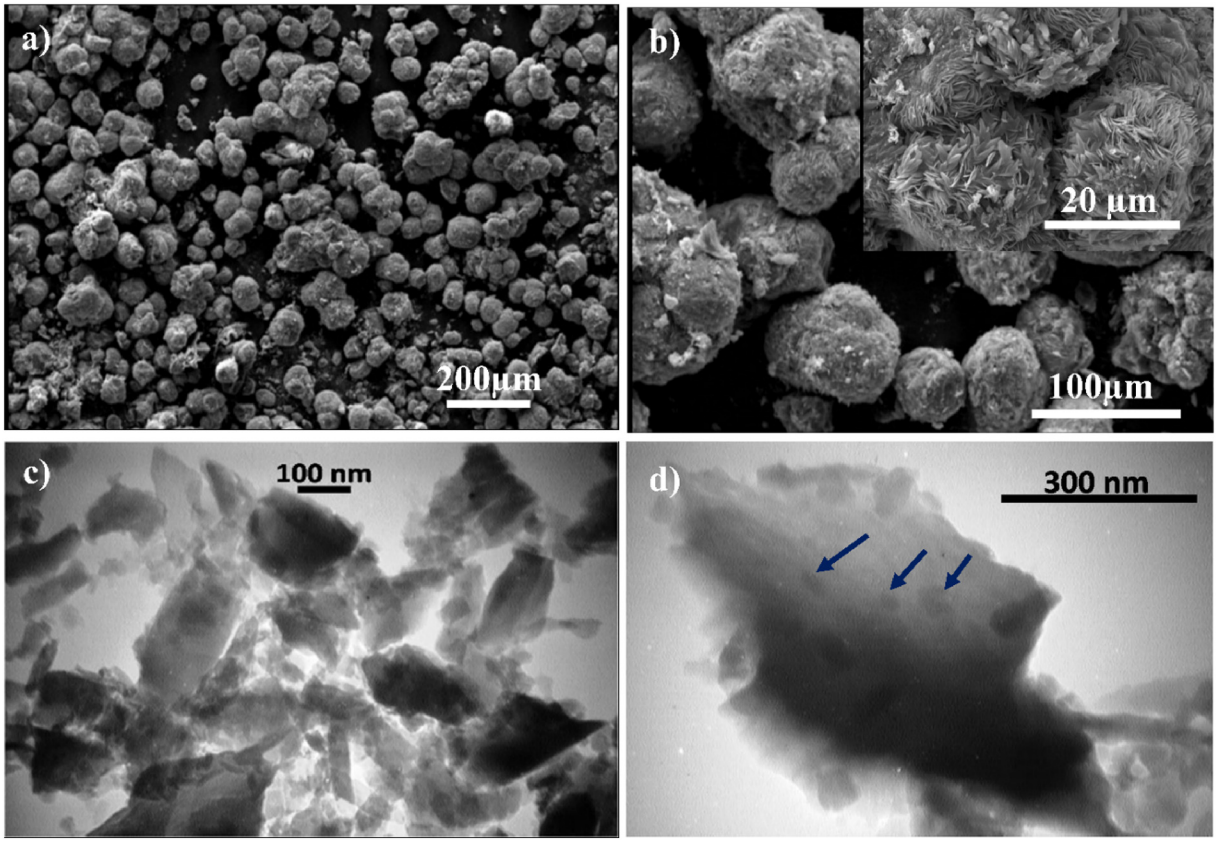

Fig. 2. SEM (a, b) and TEM images (c, d) of GO/Co-MOF sample. The blue arrow shows the Co-MOF samples decorated on the GO sheets surface. (For interpretation of the references to colour in this figure legend, the reader is referred to the web version of this article.)

Gram negative bacteria could have explained by synergistic effect between the GO sheets and Co-MOF. These results are suggested to further use of the GO/Co-MOF nanoporus hybrid for in vitro biocidal material.

2. Experimental section

2.1. Materials

1,4-Benzenedicarboxylic acid (PTA, 99.9%), $Co(NO_3)_2{\cdot}6H_2O$ (99.9%), hydrogen peroxide (H_2O_2 30%), graphite powder (mesh < 2 µm), sulfuric acid (98 wt%), acetic acid, hydrochloric acid, ethanol, *N*,*N*-dimethylformamide (DMF), sodium nitrite ($NaNO_3$), methanol and potassium permanganate ($KMnO_4$) were purchased from Merck Chemicals. DPPH was obtained from Sigma-Aldrich without any further purification.

2.2. Methods

Fourier transform infrared (FTIR) spectra were obtained on EQUINOX 55 Bruker spectrometer. The samples were prepared by grinding dried powder of GO/Co-MOF with KBr. X-ray diffraction (XRD) patterns were recorded using AXS Bruker diffractometer by Cu Kα radiation of wavelength of 0.154 nm. Ion coupled plasma optical emission spectroscopy (ICP-OES) was used to find the concentration of cobalt loading in GO/Co-MOF using Arcos instrument from Spectro. TEM images of GO/Co-MOF were utilized using Zeiss-EM10C-80 kV system. The surface morphology of GO/Co-MOF was examined by SEM (Philips, XL-30) at an accelerating voltage of 26 kV. Raman spectroscopy was utilized by Teksan (Takram, P50COR10, Iran) company with laser wavelength of 532 nm. Fluorescence microscopy of the sample was collected after adding propidium iodide (PI) and Hoechst stain from Sigma Aldrich to the GO/Co-MOF solution incubated with bacteria using Nikon, Eclipse TE2000-S system. Zeta potential was measured by Malvern Instrument Ltd-UK.

2.3. Synthesis of GO

GO was synthesized using modified Hummers' method as reported previously [60]. In summary, graphite power (0.5 g) was dispersed in 23 mL sulfuric acid. Then 0.5 g $NaNO_3$ powder was added to the solution followed by adding 3 g $KMnO_4$. The reaction was continued by stirring the mixture at 0 °C using ice bath. After 10 min, the temperate of the mixture increased to 35 °C with continues stirring for 4 h. The reaction was completed by adding 100 mL of DI water followed by adding 40 mL of DI water and 3 mL H_2O_2. The as synthesize graphite oxide was washed once using hydrochloric acid diluted by water. The final washing was done by DI water several times to control pH to 7. After washing, graphite oxide was dispersed in DI water and ultra-sonicated for 1 h with the purpose of proper exfoliation. Then, GO was dried in oven and collected for further applications.

2.4. Synthesize of the Co-MOF

The Co-MOF was synthesized via solvothermal method. In summary, a 4 mM of $Co(NO_3)_2$ and 2 mM of PTA were dissolved in 10 mL of DMF using ultra sonication. The 0.5 mL of the acetic acid are added dropwise to the solution mixture. The final pink colour solution was transferred to the Teflon-lined stainless steel and heated to 180 °C for 24 h. The resultant solution was washed by ethanol three times and dried in oven for 20 h.

2.5. Synthesis of GO/Co-MOF nanoporous hybrid

The GO/Co-MOF was synthesized by similar procedure reported for

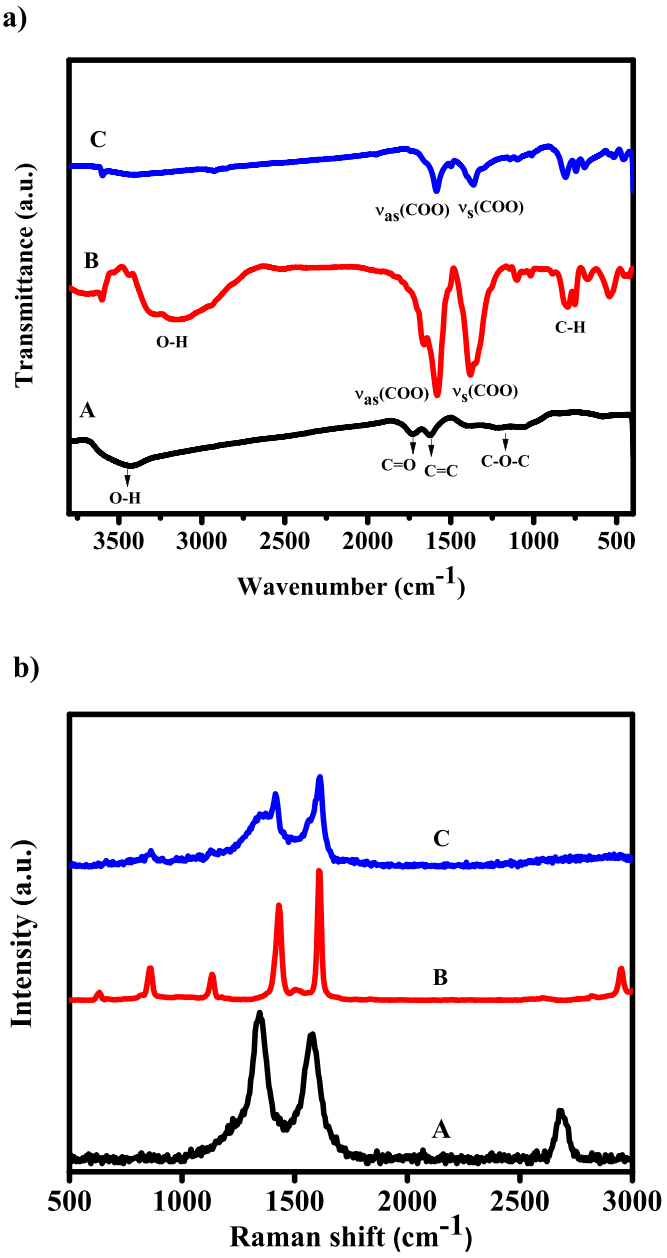

Fig. 3. FTIR (a) and Raman spectroscopy (b) of GO sheets (A), Co-MOF (B), and GO/Co-MOF nano porous hybrid.

GO hybrid nickel based MOF [61]. The 75 mg of as prepared dried GO was dissolved in DMF and stirred for 1 h. In separate flasks, 4 mM of Co $(NO_3)_2$ and 2 mM of PTA were dissolved in 10 mL of DMF using ultra sonication. Then, $Co(NO_3)_2$ solution was added to the GO solution and stirred for 2 h to complete mixing. Then, PTA was added following by addition of acetic acid. The final mixture was transferred to a 30 mL Teflon-lined stainless steel for 24 h at 180 °C. Final product was washed three times by ethanol and dried in 50 °C.

2.6. Cell viability assay

Cytotoxicity of GO/Co-MOF nanoporous hybrid was conducted using 3-[4,5-dimethylthiazol-2yl]-2,5-diphenyl tetrazolium bromide (MTT) which is a colorimetric non-radioactive assay for fibroblast cell line. About 7×10^3 cells/well of human fibroblast (Hu02) were grown in 96-well plates and cultured in Dulbecco's Modified Eagle's medium (DMEM), supplemented with 10% fetal bovine serum (FBS) and 1% penicillin at 37 °C under 5% CO_2 for 24 h, 48 h, and 72 h. Then Hu02 cells were washed with phosphate-buffered saline (PBS) and incubated with eight different concentrations of GO/Co-MOF. After 24 h of incubation, 100 μL of MTT was added into each well, followed by 3 h incubation at 37 °C under 5% CO_2. Afterwards, dimethyl sulfoxide (DMSO) was added to each well and the wells were shaken for 30 min. The optical density (OD) of each well was monitored at 570 nm using a microplate reader (Bio-Tek ELX8000). The OD at 655 nm was considered as the reference. The absorbance recorded by microplate was used for calculation of the survival cells. Data were represented as mean ± standard deviation (SD) of independent experiments.

2.7. Bacterial culture

In the antibacterial activity test, the standard bacterial strain was purchased from Iranian Biological Resource Center (IBRC) by using organism from the American Type Culture Collection (ATCC), containing Gram-negative *E. coli* (IBRC-M11018; ATCC 25922) and Gram-positive *S. aureus* (IBRC-M10690; ATCC 33591). Both bacteria were grown in Luria-Bertani (LB broth) for 24 h at 37 °C. Then the bacteria cells were centrifugation for 15 min at 5000 rpm. The collected bacterial cells were suspended in saline solution. The bacterial level for this study was 10^8 colony-forming unit (CFUs) per mL.

2.8. Antibacterial activity

Different concentrations of GO/Co-MOF nanoporous (25, 50, 75 and 100 μL) in PBS were added into the bacteria solution and the suspensions were shacked using rotary shaker at 37 °C for 2 h. Then, the solution supernatant was cultured using standard plate counted method, and the plates were incubated for 24 h at 37 °C. The number of colonies was counted for GO/Co-MOF/bacterial mixture, whereas the solution without nanoporous was counted as the control. Furthermore, the bacterial cells mixture with 100 μL of the GO/Co-MOF hybrid were stained with PI and Hoechst, and the dead and live bacterial cell were detected using fluorescence microscope. In addition, PI stain was used to label cells with compromised cellular membranes and Hoechst was used to stain DNA. In contrast, the antibacterial activities of GO and Co-MOF are also taken using same procedure.

2.9. Measurement of free radicals by DPPH assay

The DPPH assay of GO/Co-MOF extracts was measured using Campos et al. method [62]. The Hu02 fibroblast cells were treated with different concentrations of GO/Co-MOF nanoporous hybrid including 1,2,3,4 and 5 mg/mL and the amount of produced free radicals was studied using 1 mM solution of DPPH in methanol. The experimental groups of 24,48 and 72 h were incubated in dark and their absorbance in 520 nm was then read using UV–Vis spectrophotometer after 15 min. The percentage of reduced initial DPPH concentration was calculated based on Eq. (1) [63]:

$$\%\text{Absorbance (520 nm)} = 100 - [(OD_{sample} - OD_{blank}) \times 100/OD_{DPPH}] \quad (1)$$

2.10. Test for metal ion release

To investigate the release of cobalt ions from GO/Co-MOF, three samples containing 10 mg/mL of the nanoporous hybrid were dispersed in aqueous solution and shaken for 30, 90, and 120 min, each. Then the concentration of metal ions in supernatant solutions was measured using ICP-OES.

2.11. Statistical analysis

Statistical analyses were carried out using SPSS software and one-

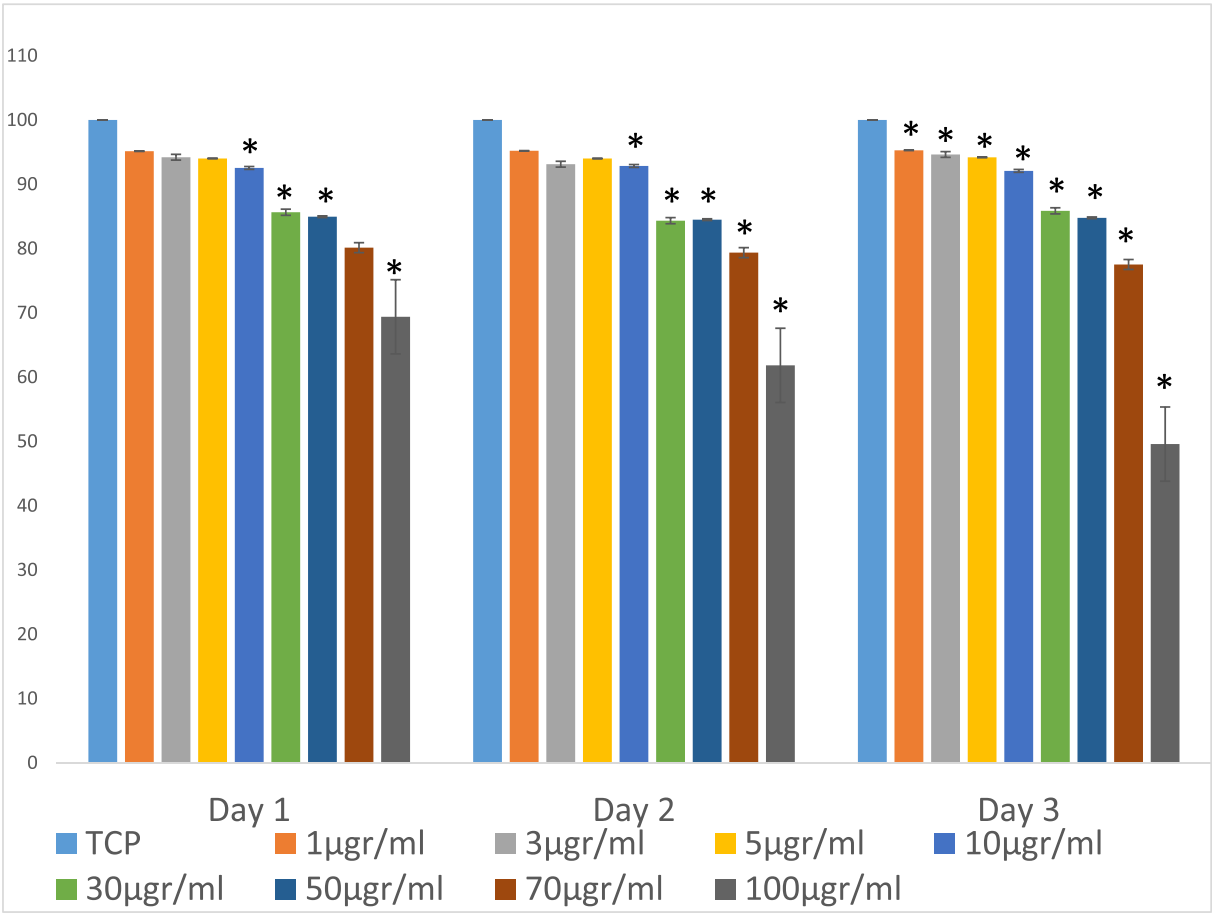

Fig. 4. MTT assay for 24, 48, 72 h using various concentration of 1, 3, 5, 10, 30, 50, 70, and 100 µg/mL of GO-Co/MOF nanoporous hybrid. The results are expressed as means ± 1 S.D. ($n = 4$).

way analysis of variance (ANOVA) is used to compare the results. For MTT assay the p value of ≤ 0.05 was considered to be statistically significant, and for DPPH assay p-values equal to 0.06, 0.187 and 0.232 were considered for 24, 48 h, and 72 h of incubation respectively. Both assays were repeated at least 4 times.

3. Results and discussion

Fig. 1Aa, Ba, and Ca shows XRD pattern of GO sheets, Co-MOF and GO/Co-MOF nanoporous hybrid respectively. The characteristic peak attributed to GO sheets (Fig. 1Aa) was appeared at $2\theta = 9.88^{\circ}$ with inter planner distance of 0.89 nm which is assigned to (002) of GO plane [46]. As shown in Fig. 2Ba, XRD pattern of Co-MOF was exhibited highly crystalline structure and characteristic peaks of typical metal organic frame work. The peak of metallic cobalt at 45°,which is corresponding to the reduction of cobalt ions (Co^{2+}) to form cobalt in the DMF solvent heated in higher temperature around 200 °C was diminished, which shows the cobalt ions are coordinated well with the PTA ligand [25,26,64]. The XRD pattern of GO/Co-MOF nanoporous hybrid also displays the highly crystalline phases of the sample, which implies that GO sheets are used as a template to arrange the Co-MOF growth. These results also illustrate that cobalt ions and PTA ligand were coordinated to make a new GO cobalt based metal organic framework [61]. In the nanohybrid synthesis process, acetic acid acts as a modulator to terminate the nanoporous hybrid crystalline structure. The inter planer distance of GO/Co-MOF nanoporous at 9.03° was calculated to be around 0.98 nm [60]. There is no characteristic peak denoted to graphene in the XRD pattern of nanoporous hybrid, which confirms that GO is not reduced during the synthesis process. Furthermore, the characteristic peak of GO sheets in the GO/Co-MOF nanoporous are strongly diminished, which is indicated the exfoliation and/or dispersion of them during synthesize process. This result also can have proved that Co-MOF are attached onto the GO surfaces without mutation of their crystal structures [61].

Zeta potential measurements of the GO sheets, Co-MOF and GO/Co-MOF nanoporous hybrid are shown in Fig. 1b. The zeta potential values of GO sheet and Co-MOF in water are measured to be −36.9 mV and −6 mV respectively. Although, the GO/Co-MOF nanoporous is revealed to have negative charge value of −21 mV. This results suggesting that, GO sheets were induced more negative charges to the Co-MOF in the GO/Co-MOF nanoporous hybrid structure.

The GO/Co-MOF morphology was seen using SEM and TEM images. As shown in SEM images (Fig. 2a,b), the cornflower like structure with a high porosity and extremely high surface area was observed. These special structures have sharp GO sheet edges in their morphology which are active parts to handle the antibacterial activity [65]. As seen in TEM images (Fig. 2c,d), the GO nanosheets are interact by Co^{2+} to provide the metal-organic coordination active centers. Here, the Co^{2+} could interact with oxygen functional group on GO nanosheet surfaces, and it can cause the Co-MOFs to be more crystalize [4]. The Co-MOFs are decorated the GO sheet surfaces as seen in Fig. 2c, d. In addition, stabilization of the Co-MOFs on the GO surfaces could avoid the agglomeration of these particles as well as restacking of the GO nanosheets and their full exfoliation. The size of GO nanosheets in the nanoporous is observed to be around 300 nm. In the synthesis process, cobalt ions are absorbed on GO sheets. The critical amount in terms of weight percentage of GO, as a metal organic framework coordinator, is affective to make more active centers in the structure. Wherein, the

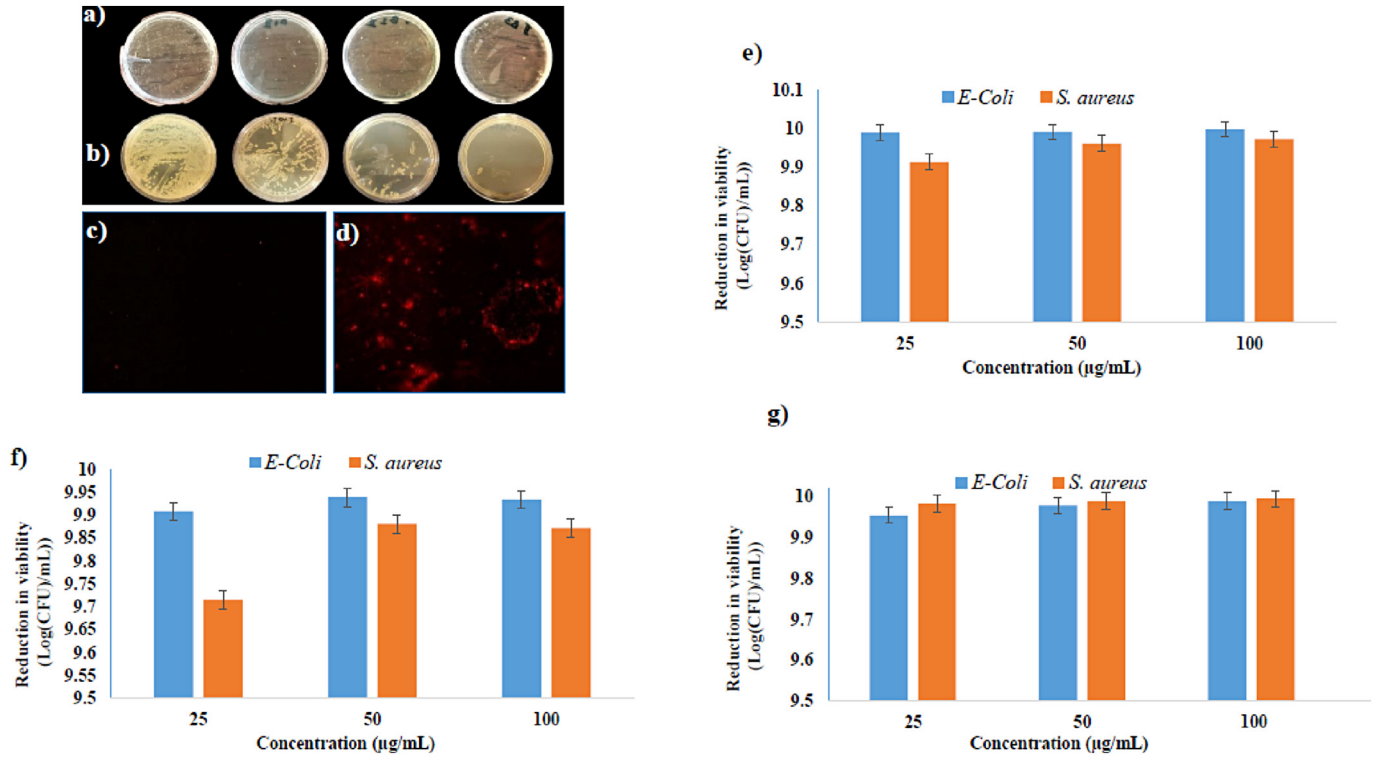

Fig. 5. Agar plate experiment to test antibacterial activity of (a) *S. aureus* and (b) *E. coli* bacteria cell. Fluorescent images of control (c) and dead bacterial cells (d) treated with 100 μg/mL of GO/Co-MOF nanoporous hybrid and the viability of *E. coli* and *S. aureus* treated with various concentration of GO (e), Co-MOF (f) and GO/Co-MOF nano porous hybrid (g).

amount of cobalt ions in the GO/Co-MOF hybrid is estimated by ICP to be around 25 wt% in the total nanoporous hybrid. As seen in the SEM images, the cornflower like structures are open and thin, which means that the Co-MOFs are formed over the surface of GO sheets, which in turn, avoids GO sheets from agglomeration and stacking. Here the Co-MOFs are estimated to be 100 nm from TEM images.

The FTIR of GO (A), Co-MOF (B), and GO/Co-MOF nanoporous hybrid (C) are shown in Fig. 3. As seen in Fig. 3Aa, the GO sheets characteristic peaks attributed to the vibration band of the epoxy is located at 1072 and 3414 cm^{-1} according to the C-O-C,O-H vibration [66]. The peak at 1733 cm^{-1} is related to the C═O bond of the carboxylic groups for the GO and the peak at 1622 cm^{-1} is associated with the C═C band of sheets. The FTIR of Co-MOF is shown in Fig. 3Ba. The strong peaks placed at 1376, and 1578 cm^{-1} are attributed to the symmetric and asymmetric stretching bands of the coordinated carboxylate group in the terephthalic acid linker respectively. The separation of strong bond for carboxylate group in terephthalic acid in two bonds, is indicated the attachments of it to the metallic cobalt via monodentate ligands. This results are confirmed the formation of cobalt hydroxyl-terephthalate-based composite. Also, the characteristic bands placed at 803, 1020, and 1105 cm^{-1} are attributed to the para-aromatic stretching bands of C—H group. The broad stretching band at 3212 cm^{-1} is assigned to the coordinated O—H of water molecules contained in the Co-MOF sample. The FTIR of GO/Co-MOF nanoporous (Fig. 3Ca) was shown the mostly same characteristic peaks as Co-MOF sample. The visible characteristic peaks of GO are not appearing proper in the GO/Co-MOF nanoporous because of high intense of Co-MOF peaks. Raman spectroscopy was used to find the number of layers and the possible disorder of graphitic structures [42]. The Raman spectra of Co-MOF (Fig. 3Bb), were exhibited the sharp peaks at 1134, 1428.3 cm^{-1} and 1608.4 cm^{-1} are attributed to in-plane vibrational of the benzene ring, and the characteristic peaks placed at 862,633.6 cm^{-1} are the out-of-plane deformation of the C—H groups in terephthalic acid.

Fig. 3Cb shows the Raman spectra of the GO/Co-MOF nanoporous hybrid material. There are two major band positions placed in 1414 and 1613 cm^{-1}, which are attributed to the D and G bonds of the hybrid material, corresponding to the κ-point phonons of A_{1g} symmetry for local defects/disorders and E_{2g} phonon of graphitic structure, respectively [46]. Both D and G peaks are upshifted to higher frequencies, which each of them handling different phenomenon. The G bond is assigned to the doped impurities in GO, which causes an increased phonon energy of graphene in the hybrid sample, which consequently decreases the intensity of the peak. The ratio of intensities of the D band to the G band (I_D/I_G), was calculated to be 0.81, for laser excitation wavelength of 532 nm.

The related in-plane crystallite size for sp^2 hybridization in the GO/Co-MOF nanoporous hybrid was calculated using equation, La (nm) = $2.4 \times 10^{-10} \times \lambda^4 \ (I_D/I_G)^{-1}$. The calculated in-plane crystal size is 23.7 nm for nanoporous hybrid which is increases in compared to that of GO sheets which is 16.6 nm. As, L_a, are shown the ordered and disordered crystal structure of carbon materials, the increase of that are attribute to the larger average sizes of crystalline graphite domains in nanoporous hybrid compared with GO [67]. It is proved that the intensity of two phonon (2D) Raman scattering band in graphene materials, which is known as adopted double resonance model, changes as a result of the stacking of graphene sheets [46].

The 2D band of the GO-based MOF hybrid shows broadened peak placed at 2794 cm^{-1}, which is upshifted compared to that of a single layered GO sheet. This confirms the multilayer structure of GO/Co-MOF (> 2–4 layers) which is in consistence with the GO multilayers shapes observed in SEM images. Also, the I_{2D}/I_G ratio of GO/Co-MOF hybrid is 0.1, which confirms multilayer structure of GO (> 4 layers). Since, the Raman pattern of GO and Co-MOF are centered in D and G and 2D bands, it can have concluded that the Co-MOFs were grown on the GO sheet surfaces.

MTT was assessed for different concentrations of GO/Co-MOF nanoporous hybrid at treatment times of 24, 48 and 72 h. As seen in Fig. 4,

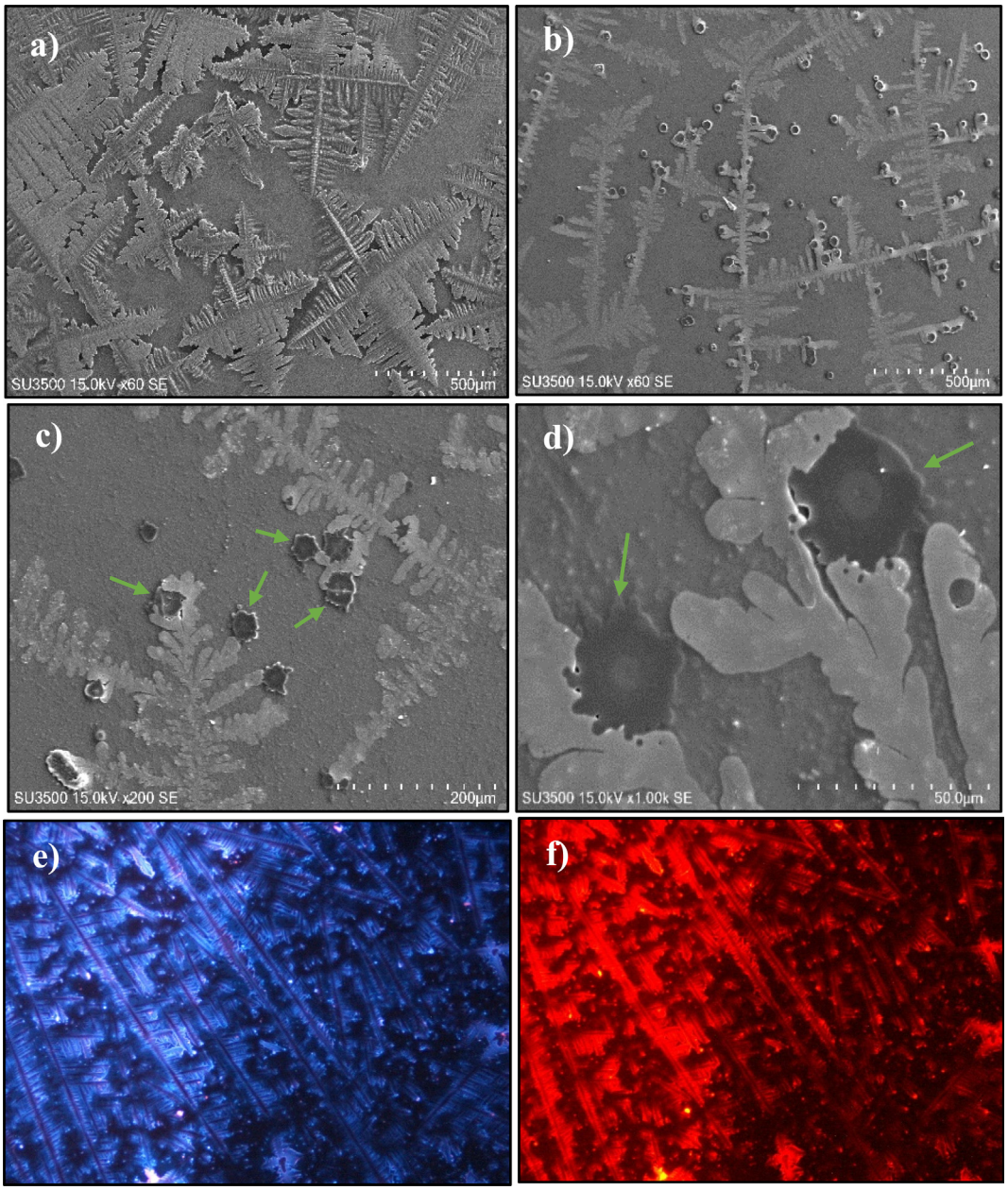

Fig. 6. SEM images of interaction of (a) control, (b–d) *E. coli* bacteria cells after exposed to 100 μg/mL of GO/Co-MOF (green arrows), (e) control bacteria stained with Hoechst (f), and PI stained of bacteria cells after exposure to 100 μg/mL of GO/Co-MOF. (For interpretation of the references to colour in this figure legend, the reader is referred to the web version of this article.)

the cell viability is over 95%, shows low toxicity in 24, 48 and 72 h in 1 μg/mL dosage of nanoporous hybrid. But at higher dosages and maximum treated time (i.e. 72 h), over 50% of the Hu02 cells would be dead [68].

Antibacterial activity of GO (e), Co-MOF (f), and GO/Co-MOF nano porous hybrid (g) were evaluated using *E. coli* and *S. aureus* as model organisms. Antibacterial activity of GO on the both bacteria was shown in Fig. 5e. As reported antibacterial activity of GO could be direct effect by their sheet sizes, which smaller sheet sizes (lateral size range of 0.01 to 0.65 μm) causes higher antibacterial activities, but the bigger sheet sizes of GO are also relevance to kill the bacteria cells as lateral GO sheet sizes could have affected their sharp edges, and their corners. Furthermore, the GO sheets thickness (single layer GO sheets exhibited more antibacterial activities compared to the multi layers), shapes (sharp edges GO sheets can damage the bacteria via affect the membrane lipid layer of the bacteria cells), surface functionality and surface coating (which can causes the wrapping of the bacteria by GO sheets and isolating them), and surface charges transfer are the important fact in their antibacterial activity [69].

Fig. 5g is shown the decrease of the cell viability in both *E. coli* and *S. aureus* cells by 99% after incubation with GO/Co-MOF suspension for 2 h. In the control bacteria without nano porous GO/Co-MOF, no dead cells were observed. The GO/Co-MOF shows stronger antibacterial activity in *S. aureus* bacterial than in *E. coli*. It is reported which cobalt based MOFs (Co-MOF) are too much affective toward Gram-positive bacteria (*Staphylococcus aureus*), because these bacteria cells have lipoteichoic acid in their peptidoglycan layer which can act as chelating agents to prevention lipid peroxidation, which causes to bacteria cell membrane damage through lipid peroxidation [35,70].

As reported, agglomeration of graphene sheets could decrease their anti-bacterial activities. Here, in the flower shape in the nano porous hybrid structure the GO sheets are stick together using PTA linker

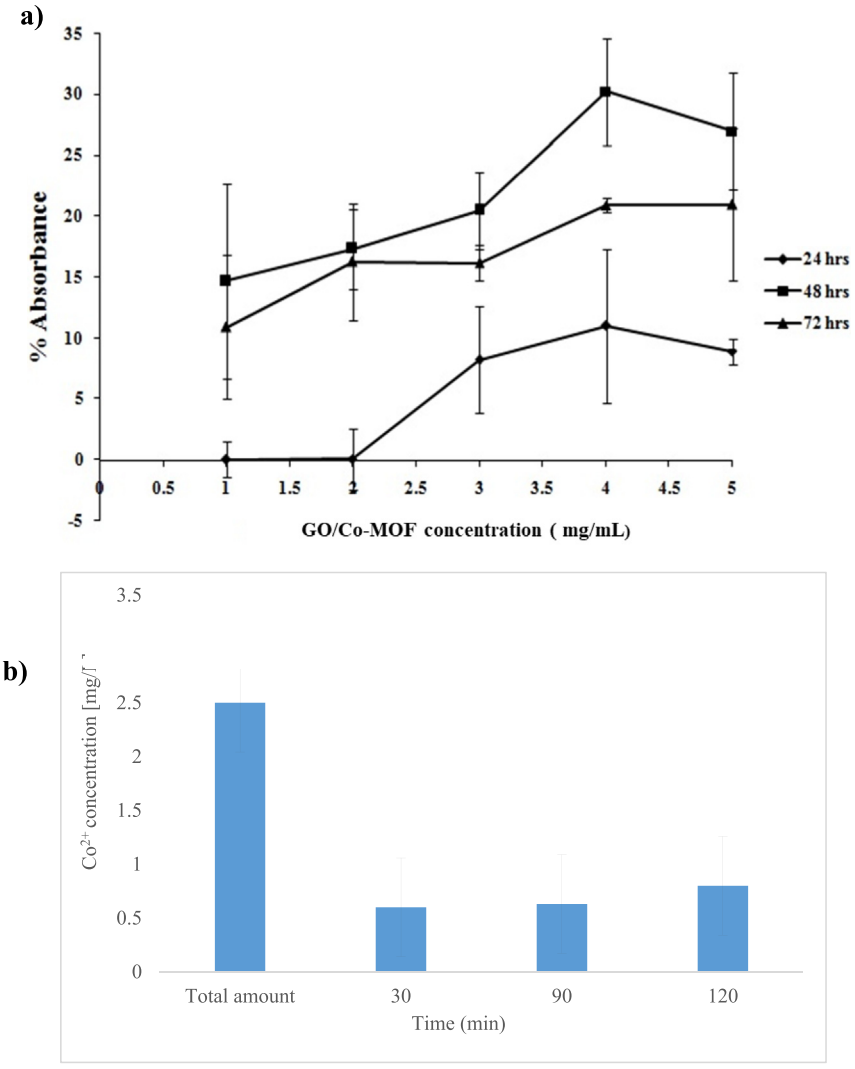

Fig. 7. (a) DPPH test of free radical release, *p*-values = 0.06, 0.187 and 0.232 for 24, 48 h, and 72 h, respectively, and (b) ICP results of cation release from different time duration of 30, 90, and 120 min from initial amount of 2.5 mgL^{-1} of GO-Co/MOF.

which avoids agglomeration of them. Therefore, even at a low concentration of 25 μg/mL of GO/Co-MOF, the bacterial vitality showed higher decrease. As compared to the antibacterial activity of GO (with the size of 1.5 μm) and Co-MOF (with the size of 50 μm) (Fig. 5e, f), their combination in the form of GO/Co-MOF shows better antibacterial activities indeed. The plating counted bacteria for *E. coli* and *S. aureus* bacteria for the GO/Co-MOF are shown in the Fig. 5a, b. As shown in the Figure the bacteria viability of the nanoporous hybrid was decreased by increasing the concentration of GO/Co-MOF.

This results were confirmed the inhibiting of bacterial colony and the antibacterial activity potential on Gram-negative and Gram-positive bacteria. There are two different phenomenon of the interaction of the GO/Co-MOF with bacteria. To find the type of interaction of GO/Co-MOF with bacteria, as to be either attached to the bacteria cells structure or up taken in the bacterial cells, SEM images were taken. The SEM images clearly show that GO/Co-MOF, sharp edges are responsible for the damage of bacterial cells. The GO/Co-MOF nanoporous hybrid scratches the bacterial cell walls and initiates destroying of their cells membranes, as shown in the Fig. 6(a–d). The SEM images also show bacterial cell injury, leading to stress formation on the bacterial cell walls. Since GO/Co-MOF has not entered into the bacterial cells, due to agglomeration an increase was observed in the size of the GO/Co-MOF nanoporous hybrid, while the GO edges and functional oxygen on their surfaces are responsible for antibacterial activity [71]. Fig. 6e and f shows that the majority of dead cells are incubated by 100 μL of GO/Co-MOF hybrid.

The generated radicals from cultured cells which were treated by GO/Co-MOF nanoporous hybrid were measured through scavenging of DPPH free radicals. The measurements were done for neat GO/Co-MOF and nanoporous hybrid was incubated with cells. As obtained from absorbance at 520 nm based on Eq. (1), the higher value of OD_{sample} confirms the lower produced radicals as a result of the treatment of the GO/Co-MOF nanoporous hybrid [72]. Accordingly, the associated results illustrate no considerable difference between various concentrations. As shown in the Fig. 7a, the cells were not able to quench DPPH as a function of produced radicals [63]. Thus, there is no radical mediated toxicity with the corresponding nanoporous hybrid. Finally, to investigate the contribution of the free cobalt ions on the antibacterial activity of the samples, their release was investigated using ICP-OES for the three time durations. As shown in the Fig. 7b, the Co^{2+} concentrations in the aqueous media were increased to be 0.6, 0.63, and 0.8 mg/L respectively via releasing time. The increasing of the metal cations is probably caused by cobalt ions which are detached from the GO/Co-MOF nanoporous hybrid surfaces. Furthermore, possible mechanism for antibacterial activity of GO/Co-MOF nanoporous hybrid are proposed to be the synergistic antimicrobial effect of GO sheets and Co-MOF composite. The Co-MOF composite has chemical reactivity and extremely superior amount of the cobalt surface element,

which its antibacterial activity was created via releasing of the metal ions (Co^{2+}) which can interact with bacteria membrane [35].

In addition, the common phenomena of antimicrobial inactivation were investigated to be corresponding to the several reason [35] which are summarized as damage of bacteria cell wall via (i) lipid peroxidation, and (ii) direct interaction of the cobalt ions (Co^{2+}) in the Co-MOF composite with the phosphate anion (such as PO_4^{3-}) at the bacteria phospholipid membrane and the interaction of the carboxylate group of Co-MOF with the Ca^{2+} and Mg^{2+} cation in the bacteria cell nutrient medium, which this interactions can causes generation of a reactive oxygen species (ROS) on their the cytoplasmic membrane which can mechanically damage the bacteria cell walls [73]. Also, cation transport interruption could happen because of the interaction of the composite with the phospholipid layer in bacteria cells which led to a disruption of cation storage and membrane homeostasis which kill the bacteria cell. In addition, bacteria cells tune to chelating metals such as cobalt, which are toxic for them. Membrane depolarization which is regarding the interaction between particles and membrane, can occurred formation of ion channels, between the inner and outer side of bacteria cell membrane which is reported for Gram-negative bacteria, via monovalent cations around their cytoplasmic membrane [74,75]. In other part, GO sheet also have potential in antibacterial activity which can interact with the bacteria lipid and protein membrane via electrostatic bonding (having highly negative charge), hydrogen bonding and their Van der Waals and π-π stacking interaction (having π-conjugated structure) [76,77]. Also, GO sheets can capture the bacteria cell and wrap and isolated them. In addition, physical damage by GO sharp edges on bacteria cells can ruptured of the bacteria cytomembrane [78]. Here, the antibacterial activity is proving to be the combination of the effect of GO sheets and Co-MOF composite of GO/Co-MOF nanoporous hybrid.

4. Conclusion

In this research, GO/Co-MOF nanoporous hybrid was synthesized and its antibacterial activities toward *E. coli* and *S. aureus* bacteria was studied and compared at different concentrations of them. The antibacterial mechanism was discussed in terms of bacteria membrane damaging GO and cobalt ion release. Results of colony counting show the extremely high antibacterial activities of GO/Co-MOF against both bacteria, though more significantly on *S. aureus* at equal bacteria concentrations. Furthermore, the bacteria inactivation rate increased as a result of increasing of hybrid concentration, which can be described to be due to higher concentration of sharp GO edges and higher oxygen functional groups. In consequence, the GO/Co-MOF nanoporous hybrid is capable of being employed in antibacterial applications.

Acknowledgement

The authors would like to thank Ministry of Science and Technology (Grants MOST 105-2628-M-007-002-MY3, MOST 104-2221-E-007-015-MY4).

References

[1] M. Giménez-Marqués, T. Hidalgo, C. Serre, P. Horcajada, Nanostructured metal-organic frameworks and their bio-related applications, Coord. Chem. Rev. (2015) 1–19.
[2] A.C. McKinlay, et al., BioMOFs: metal-organic frameworks for biological and medical applications, Angew. Chem. Int. Ed. 49 (36) (2010) 6260–6266.
[3] S. Keskin, S. Kizilel, K. Seda, S. Kızılel, Biomedical applications of metal organic frameworks, Science 50 (4) (2010) 1799–1812.
[4] P. Horcajada, R. Gref, T. Baati, P.K. Allan, G. Maurin, P. Couvreur, Metal À Organic Frameworks in Biomedicine, (2012), pp. 1232–1268.
[5] K.M.L. Taylor, W.J. Rieter, W. Lin, Manganese-based Nanoscale Metal-organic Frameworks for Magnetic Resonance Imaging, (2008), pp. 14358–14359.
[6] J.E. Mondloch, O. Karagiaridi, O.K. Farha, J.T. Hupp, Activation of Metal–Organic Framework Materials, (2013), pp. 9258–9264.
[7] A. Dhakshinamoorthy, A.M. Asiri, H. Garcia, Metal-organic frameworks catalyzed C-C and C-heteroatom coupling reactions, Chem. Soc. Rev. 44 (7) (2015) 1922–1947.
[8] D. Farrusseng, S. Aguado, C. Pinel, Minireviews MOFs in Catalysis Metal–Organic Frameworks: Opportunities for Catalysis, (2009), pp. 7502–7513.
[9] J. An, S.J. Geib, N.L. Rosi, High and selective CO_2 uptake in a cobalt adeninate metal-organic framework exhibiting pyrimidine- and amino-decorated pores, J. Am. Chem. Soc. 132 (1) (2010) 38–39.
[10] S. Fardindoost, S. Hatamie, A.I. Zad, F.R. Astaraei, Hydrogen sensing properties of nanocomposite graphene oxide/Co-based metal organic frameworks (Co-MOFs@GO), Nanotechnology 29 (1) (2018).
[11] N. Motakef-kazemi, S. Abbas, A. Morsali, Microporous and mesoporous materials in situ synthesis of a drug-loaded MOF at room temperature, Microporous Mesoporous Mater. 186 (2014) 73–79.
[12] P. Horcajada, et al., Porous metal–organic-framework nanoscale carriers as a potential platform for drug delivery and imaging, Nat. Mater. 9 (2) (2010) 172–178.
[13] K.L. Mulfort, J.T. Hupp, Alkali metal cation effects on hydrogen uptake and binding in metal-organic frameworks, Society 47 (18) (2008) 7936–7938.
[14] S. Lin, et al., Porous Iron-Carboxylate Metal–Organic Framework: A Novel Bioplatform with Sustained Antibacterial Efficacy and Nontoxicity, vol. 53, (2017).
[15] M. Berchel, et al., A silver-based metal–organic framework material as a 'reservoir' of bactericidal metal ions, New J. Chem. 35 (2011) 1000–1003.
[16] X. Wang, D. Zhao, A. Tian, J. Ying, Three 3D silver-bis(triazole) metal-organic frameworks stabilized by high-connected Wells-Dawson polyoxometallates, Dalton Trans. (2014) 5211–5220.
[17] M. Pilar, et al., Coatings Surface Anchored Metal-Organic Frameworks as Stimulus Responsive Antifouling Coatings, vol. 29, (2015) no. 2013.
[18] A.R. Abbasi, K. Akhbari, A. Morsali, Ultrasonics sonochemistry dense coating of surface mounted CuBTC metal–organic framework nanostructures on silk fibers, prepared by layer-by-layer method under ultrasound irradiation with antibacterial activity, Ultrason. Sonochem. 19 (4) (2012) 846–852.
[19] Y. Zhou, Z. Mao, W. Wang, Z. Yang, X. Liu, In-Situ Fabrication of Graphene Oxide Hybrid Ni-Based Metal–Organic Framework (Ni–MOFs @ GO) with Ultrahigh Capacitance as Electrochemical Pseudocapacitor Materials, (2016).
[20] T. Action and J. Snow, "On Chloroform and Other Anesthetics," pp. 42–46.
[21] P. Taylor, A.K. Mahapatra, K. Muthukumarappan, J.L. Julson, Applications of Ozone, Bacteriocins and Irradiation in Food Processing: A Review Applications of Ozone, Bacteriocins and Irradiation in Food Processing, August 2013 (2007), pp. 37–41.
[22] W.H. Glaze, J. Kang, H. Douglas, Ozone: science & engineering the chemistry of water treatment processes involving ozone, hydrogen peroxide and ultraviolet radiation, Ozone Sci. Eng. 2011 (August) (2008) 335–352.
[23] M.A. Butkus, L. Edling, M.P. Labare, M.P. Labare, The Efficacy of Silver as a Bactericidal Agent: Advantages, Limitations and Considerations for Future Use, August (2018), pp. 407–416.
[24] S. Hatamie, S.D. Dhole, J. Ding, S.N. Kale, Journal of Magnetism and Magnetic Materials Encapsulation of Cobalt Nanoparticles in Cross-linked-polymer Cages, 321 (2009), pp. 2135–2138.
[25] S. Hatamie, M.V. Kulkarni, S.D. Kulkarni, R.S. Ningthoujam, R.K. Vatsa, S.N. Kale, Cobalt nanoparticles doped emaraldine salt of polyaniline: a promising room temperature magnetic semiconductor, J. Magn. Magn. Mater. 322 (24) (2010).
[26] S. Hatamie, M.M. Ahadian, A. Rashidi, A. Karimi, O. Akhavan, Novel synthesis of cobalt/poly vinyl alcohol/gamma alumina nanocomposite for catalytic application, Appl. Phys. A Mater. Sci. Process. 123 (5) (2017).
[27] S. Gupta, S.M. Nalawade, S. Hatamie, H.V. Thakur, S.N. Kale, Sensitive, weak magnetic field sensor based on cobalt nanoparticles deposited in micro-tunnels of PM-PCF optical fiber, AIP Conference Proceedings, vol. 1391, 2011.
[28] K. Awazu, M. Fujimaki, C. Rockstuhl, and J. Tominaga, "A Plasmonic Photocatalyst Consisting of Silver Nanoparticles Embedded in Titanium Dioxide," no. vol. 4, pp. 1676–1680, 2008.
[29] H.S. Rodríguez, J.P. Hinestroza, C. Ochoa-Puentes, C.A. Sierra, C.Y. Soto, Antibacterial activity against Escherichia coli of Cu-BTC (MOF-199) metal-organic framework immobilized onto cellulosic fibers, J. Appl. Polym. Sci. 131 (19) (2014) 1–5.
[30] S. Hatamie, V. Dhas, B. B. Kale, I. S. Mulla, and S. N. Kale, "Author's Personal Copy Polymer-embedded Stannic Oxide Nanoparticles as Humidity Sensors."
[31] M. Moritz, M. Geszke-Moritz, The newest achievements in synthesis, immobilization and practical applications of antibacterial nanoparticles, Chem. Eng. J. 228 (2013) 596–613.
[32] G. Wyszogrodzka, B. Marszałek, B. Gil, P. Doroz, Metal–Organic Frameworks: Mechanisms of Antibacterial Action and Potential Applications, vol. 21, (2016) no. 6.
[33] A. Carné, C. Carbonell, I. Imaz, D. Maspoch, Nanoscale metal-organic materials, Chem. Soc. Rev. 40 (1) (2011) 291–305.
[34] S. Aguado, J. Quirós, J. Canivet, D. Farrusseng, K. Boltes, R. Rosal, Antimicrobial activity of cobalt imidazolate metal-organic frameworks, Chemosphere 113 (2014) 188–192.
[35] W. Zhuang, D. Yuan, J. Li, Z. Luo, H. Zhou, Highly Potent Bactericidal Activity of Porous Metal–Organic Frameworks, (2012), pp. 225–238.
[36] A. Alonso, X. Mu, J. Macan, M. Mu, J. Mas, D.N. Muraviev, Characterization of Fibrous Polymer Silver/Cobalt Nanocomposite with Enhanced Bactericide Activity, (2012), pp. 783–790.
[37] A. Borenstein, O. Hanna, R. Attias, S. Luski, Carbon-based Composite Materials for Supercapacitor Electrodes: A Review, (2017), pp. 12653–12672.
[38] R. Banerjee, H. Furukawa, D. Britt, C. Knobler, M.O. Keeffe, O.M. Yaghi, Control of Pore Size and Functionality in Isoreticular Zeolitic Imidazolate Frameworks and Their Carbon Dioxide Selective Capture Properties, (2009), pp. 3875–3877.

[39] Z.S. Hosseini, A. Iraji Zad, M.A. Ghiass, S. Fardindoost, S. Hatamie, A new approach to flexible humidity sensors using graphene quantum dots, J. Mater. Chem. C 5 (35) (2017).
[40] S. Fardindoost, A.I. Zad, Z.S. Hosseini, S. Hatamie, Detecting hydrogen using graphene quantum dots/WO_3 thin films, Mater. Res. Express 3 (11) (2016).
[41] V. Shirshahi, S. Hatamie, S.N. Tabatabaei, M. Salimi, R. Saber, Enhanced thermal stability and biocompatibility of gold nanorods by graphene oxide, Plasmonics 13 (2017) 1585–1594.
[42] O. Akhavan, E. Ghaderi, E. Abouei, S. Hatamie, E. Ghasemi, Accelerated differentiation of neural stem cells into neurons on ginseng-reduced graphene oxide sheets, Carbon N. Y. 66 (2014).
[43] M. Mahmoudifard, M. Soleimani, S. Hatamie, S. Zamanlui, and P. Ranjbarvan, "The different fate of satellite cells on conductive composite electrospun nanofibers with graphene and graphene oxide nanosheets," Biomed. Mater., vol. 025006, p. 25006.
[44] V. Shirshahi, S. Nasrollah, S. Hatamie, R. Saber, Journal of pharmaceutical and biomedical analysis functionalized reduced graphene oxide as a lateral flow immunoassay label for one-step detection of Escherichia coli O157: H7, J. Pharm. Biomed. Anal. 164 (2019) 104–111.
[45] S. M. Ghafary, S. Hatamie, M. Nikkhah, and S. Hosseinkhani, "The Effect of Graphite Sources on Preparation of Photoluminescent Graphene Nano-sheets for Biomedical Imaging," vol. 4, no. 3, pp. 164–169, 2017.
[46] S. Hatamie, et al., Graphene/cobalt nanocarrier for hyperthermia therapy and MRI diagnosis, Colloids Surf. B Biointerfaces 146 (2016).
[47] S. Hatamie, et al., Complexes of cobalt nanoparticles and polyfunctional curcumin as antimicrobial agents, Mater. Sci. Eng. C 32 (2) (2012).
[48] E. Esmaeili, S. Hatamie, and S. Vakilian, "Magnetoelectric Nanocomposite Scaffold for High Yield Differentiation of Mesenchymal Stem Cells to Neural-like Cells," no. November 2018, pp. 1–12, 2019.
[49] Y. Chen, Y. Hsueh, C. Hsieh, D. Tzou, and P. Chang, "Antiviral Activity of Graphene–Silver Nanocomposites Against Non-enveloped and Enveloped Viruses," pp. 4–6.
[50] H. Nazari, et al., Fabrication of graphene-silver/polyurethane nanofibrous scaffolds for cardiac tissue engineering, Polym. Adv. Technol. (April) (2019) 4641 pat.
[51] O. Akhavan, E. Ghaderi, Photocatalytic Reduction of Graphene Oxide Nanosheets on TiO_2 Thin Film for Photoinactivation of Bacteria in Solar Light Irradiation, no. 50 mL (2009), pp. 20214–20220.
[52] W. Zhang, et al., Functionalization of ultra fi ltration membrane with polyampholyte hydrogel and graphene oxide to achieve dual antifouling and antibacterial properties, J. Membr. Sci. 565 (July) (2018) 293–302.
[53] C. Shuai, et al., A graphene oxide-Ag co-dispersing nanosystem: dual synergistic effects on antibacterial activities and mechanical properties of polymer scaffolds, 347 (April) (2018) 322–333.
[54] Y. Zheng, S. Zheng, H. Xue, H. Pang, Metal-Organic Frameworks/Graphene-based Materials: Preparations and Applications, vol. 1804950, (2018), pp. 1–28.
[55] Y. Wang, C. Hou, Y. Zhang, F. He, M. Liu, and X. Li, "PDA/MOF Microcapsules with Immobilized System for Electrochemical Sensing of Glucose," pp. 3695–3702, 2016.
[56] V. Jabbari, J.M. Veleta, M. Zarei-chaleshtori, J. Gardea-torresdey, D. Villagrán, Green synthesis of magnetic MOF @ GO and MOF @ CNT hybrid nanocomposites with high adsorption capacity towards organic pollutants, Chem. Eng. J. 304 (2016) 774–783.
[57] Y. Tang, S. Zheng, Y. Xu, X. Xiao, H. Xue, H. Pang, Advanced batteries based on manganese dioxide and its composites, Energy Storage Mater. 12 (February) (2018) 284–309.
[58] P. Yang, Q. Liu, J. Liu, (UiO-66) on Functionalized Graphene Oxide (GO) As, (2017), pp. 17933–17942.
[59] X. Hao, Z. Jin, H. Yang, G. Lu, Y. Bi, Applied catalysis B: environmental peculiar synergetic effect of MoS_2 quantum dots and graphene on metal-organic frameworks for photocatalytic hydrogen evolution, Appl. Catal. B Environ. 210 (2017) 45–56.
[60] S. Hatamie, O. Akhavan, S.K. Sadrnezhaad, M.M. Ahadian, M.M. Shirolkar, H.Q. Wang, Curcumin-reduced graphene oxide sheets and their effects on human breast cancer cells, Mater. Sci. Eng. C 55 (2015).
[61] Y. Zhou, Z. Mao, W. Wang, Z. Yang, X. Liu, In-situ fabrication of graphene oxide hybrid Ni-based metal-organic framework (Ni-MOFs@GO) with ultrahigh capacitance as electrochemical pseudocapacitor materials, ACS Appl. Mater. Interfaces 8 (42) (2016) 28904–28916.
[62] L. M. A. S. De Campos, F. V Leimann, R. Curi, and S. R. S. Ferreira, "Bioresource Technology Free Radical Scavenging of Grape Pomace Extracts from Cabernet Sauvingnon (*Vitis vinifera*)," vol. vol. 99, pp. 8413–8420, 2008.
[63] Y. U. Y. Amasaki, E. R. A. Nuurad, K. U. S. Hiwaku, and Y. O. Y. Amane, "Screening for Antioxidant Activity in Edible Plant Products: Comparison of Low-Density Lipoprotein Oxidation Assay, DPPH Radical Scavenging Assay, and Folin－Ciocalteu Assay."
[64] S. Hatamie, S.D. Dhole, J. Ding, S.N. Kale, Encapsulation of cobalt nanoparticles in cross-linked-polymer cages, J. Magn. Magn. Mater. 321 (14) (2009).
[65] S. Liu, et al., Lateral Dimension-dependent Antibacterial Activity of Graphene Oxide Sheets, (2012).
[66] M. Mahmoudifard, et al., The different fate of satellite cells on conductive composite electrospun nanofibers with graphene and graphene oxide nanosheets, Biomed. Mater. 11 (2) (2016).
[67] W. Niu, Y. Yang, Amorphous MOF Introduced N-doped Graphene: An Efficient and Versatile Electrocatalyst for Zinc－Air Battery and Water Splitting, (2018).
[68] C. Tamames-Tabar, et al., Cytotoxicity of nanoscaled metal–organic frameworks, J. Mater. Chem. B 2 (3) (2014) 262–271.
[69] A. Fonseca, S. Nejati, M. Elimelech, E. Engineering, N. Haven, U. States, Antimicrobial Properties of Graphene Oxide Nanosheets: Why Size Matters, no. 7 (2015), pp. 7226–7236.
[70] S. Morein, A.S. Andersson, L. Rilfors, G. Lindblom, Wild-type Escherichia coli cells regulate the membrane lipid composition in a 'window' between gel and non-lamellar structures, J. Biol. Chem. 271 (12) (1996) 6801–6809.
[71] X.Q. Dou, D. Zhang, C. Feng, L. Jiang, Bioinspired hierarchical surface structures with tunable wettability for regulating bacteria adhesion, ACS Nano 9 (11) (2015) 10664–10672.
[72] K. Sowndhararajan, S.C. Kang, Free radical scavenging activity from different extracts of leaves of Bauhinia vahlii Wight & Arn, Saudi J. Biol. Sci. 20 (4) (2013) 319–325.
[73] C.P. Moorhouse, B. Halliwell, M. Grootveld, J.M.C. Gutteridge, Cobalt (II) ion as a promoter of hydroxyl radical and possible 'crypto-hydroxyl' radical formation under physiological conditions. Differential effects of hydroxyl radical scavengers, BBA-Gen. Subjects 843 (3) (1985) 261–268.
[74] C. Ranquet, S. Ollagnier-de-Choudens, L. Loiseau, F. Barras, M. Fontecave, Cobalt stress in Escherichia coli: the effect on the iron-sulfur proteins, J. Biol. Chem. 282 (42) (2007) 30442–30451.
[75] S. Jang, J.A. Imlay, Hydrogen peroxide inactivates the Escherichia coli Isc iron-sulphur assembly system, and OxyR induces the Suf system to compensate, Mol. Microbiol. 78 (6) (2010) 1448–1467.
[76] E. Akbari, O. Akhavan, S. Hatamie, R. Rahighi, SC, J. Drug Deliv. Sci. Technol. 45 (2018) 422–427.
[77] S.M. Ghafary, M. Nikkhah, S. Hatamie, S. Hosseinkhani, Simultaneous gene delivery and tracking through preparation of photo-luminescent nanoparticles based on graphene quantum dots and chimeric peptides, Sci. Rep. (2017) 1–14 no. March.
[78] S. Gurunathan, J.W. Han, V. Eppakayala, J.H. Kim, Microbial reduction of graphene oxide by Escherichia coli: a green chemistry approach, Colloids Surf. B Biointerfaces 102 (2013) 772–777.